Original Research Paper

Radar Cross Section Modelling and Analysis of Static and Dynamic Targets using MATLAB

Punam Pande, Sreemathy R and Mousami Turuk

Department of Electronics and Telecommunication Engineering, Pune Institute of Computer Technology, Pune, India

Abstract: Radar Cross Section (RCS) is an important characteristic of the electromagnetic system for target detection. This study presents detailed modelling of Radar Cross Section (RCS) of static simple objects like sphere, cylinder, triangular plate, circular flat plate, truncated cone, and complex objects using MATLAB Radar toolbox. The RCS modelling of simple objects is also done with MATLAB POFACET GUI 4.3 and the results are compared with the MATLAB Radar toolbox. The RCS of complex objects are vectorially added in MATLAB and modelled in this work. Modelling includes 1. A cylinder with a circular flat plate on both ends 2. A circular cylinder with ellipsoid at front end 3. A truncated cone (frustum) with circular plates at both ends 4. The half ellipsoid with a frustum and the flat plate. The simulation and comparison of the RCS variations in DBSM with respect to aspect angle for parameters such as size and frequency of the simple and complex objects have been carried out in this study. RCS of a complex object with dynamic characteristics is also analysed using the Chi-square probability density function. 'The scope of this study is limited to the objects with deterministic shapes and the combined objects using those shapes. The detailed experimental study on the sphere shows that RCS remains constant in all directions for the sphere. The study also highlights the RCS return is maximum at 180 degrees when the cylinder is aligned horizontally with the RADAR and the minimum RCS is obtained at 90 degrees and 270 degrees. In the case of an ellipsoid, the RCS is maximum at 90 degrees and 270 degrees and minimum at 180 degrees. For the triangular flat plate, the RCS is maximum at 0 degrees and 180 degrees and minimum at 90 degrees. For the truncated cone the RCS has maximum and minimum values at aspect angles of zero degrees and 80 degrees. The model of the frustum with a flat plate at both ends provides maximum RCS due to the frustum and minimum due to flat plate and the normal incidence occurs at 73.3008 degrees. The Swerling models for the fluctuating RCS are also analysed in detail which will be used to measure the RCS of high-speed debris revolving around the earth's surface by the radar in Low Earth Orbit (LEO).

Keywords: Radar Cross Section Modelling, Elevation Angle, Simple and Complex Targets, Swerling Models

Introduction

Radar Cross Section (RCS) is a measure of area when the energy is incident on target from radar. The required information for tracking a target is embedded complexly in measured RCS. The RCS varies with different parameters like frequency, range shape and polarization.

Radar Cross Section is defined as:

$$\sigma = \lim_{x \to \infty} 4\pi R^2 \frac{|Es|^2}{|Ei|^2} \qquad (1)$$

where, *Ei* is transmitted Electric Field (EF) intensity and *Es* is backscattered energy. *R* is the target distance from radar and σ is measured RCS.

The important characteristic of a radar system is to detect and analyze the shape, range, effective capture area

Science Publications

and size of an object. Radar tracking efficiency is determined by the target Radar Cross Section (RCS), which is highly dependent on both target features and radar parameters (Surender *et al.*, 2021). Also, RCS estimation and modeling of the pre-launch vehicle for its real-time trajectory is designed. The intensity of backscattered RCS from a target is proportional to the ratio of the size of the object to the wavelength (Skolnik, 1970). RCS predictions are very complex even for a simple object with exact methods.

The important RCS prediction techniques are categorized as Exact Methods and Approximate methods. The exact methods involve solving differential and integral equations for certain boundary conditions based on Maxwell's equations for a given target. The exact methods are MOM (Method of Moments), FD-TD (Finite Difference Time Domain Method) and Finite Element Method (FEM The detailed analysis of tunnel using FEM method is addressed with MATLAB codes by Afrazi *et al.* (2017). Approximate methods find the solution for predicting the RCS of complex and large targets such as ships, aircraft and missiles. The most commonly defined approximate methods are Geometrical Theory of Diffraction (GTD), Physical Theory of Diffraction (PTD), Geometrical Optics (GO), Physical Optics (PO) and Method of Equivalent Currents (MEC) (Skolnik, 1970; Merrill, 2001; Mahafza;2005). The PO (physical optics) approximation for monostatic Radar Cross Section proves efficient as the approximated values do not differ much from the more exact ones (Emhemmed *et al.*, 2019). RCS can be modeled by simple equations for any shape of targets as a function of height of objects to the ground using various simulation tools is discussed in (Divyalakshmi *et al.*, 2018). The RCS measurement based on point scatter modeling for larger radar cross section is discussed in (Ahmed and Mirghani, 2018). Targets having bright illumination and continuous scattering from their surface are modeled easily with a point scatter model. The Physical Optics (PO) methods provide good results in high-frequency regions of large size targets for specular return (Chibuisi, 2015). Researchers have analyzed the Radar Cross Section (RCS) of an integrated mast and present the optimized mast shape for RCS reduction for the RCS of a naval ship equipped with the integrated mast have been analyzed (Shin *et al.*, 2021). Radar Cross Section of Orbital Debris Objects is performed with the radar-data analysis using the model Orbital Debris (OD) populations in the near-Earth environment, focusing on Radar Cross Section (RCS) (Xu *et al.*, 2019). Hence, the Radar Cross Section (RCS) analysis is crucial at the transmitter side of the Radar system with the use of computer simulation software.

The brief review and analysis of simple objects are done using standard equations from (Mahafza, 2005), whereas complex objects are simulated and discussed in

detail in the presented work. The Swerling models for the fluctuating RCS are also analyzed in depth. This type of models may be applicable to measure RCS of high-speed debris revolving around the earth's surface by the radar in Low Earth Orbit (LEO).

The launched satellites are revolving in different orbits. The satellites become nonfunctional after a prolonged period of revolution in the orbits. The satellite may be damaged due to the collisions. Hence, detailed study of RCS of these objects are essential. RCS study may be helpful in the life time assessment of the revolving unfunctional satellites.

Materials and Methods

RCS analysis for complex objects is done with Radar toolbox. Radar toolbox in MATLAB involves algorithms and tools for designing, simulating, analyzing and testing multifunction radar systems. The comparison of the study is done with MATLAB and POFACET GUI. The GUI of POFACET has the flexibility to change all the dimensions of the objects and parameters like frequency, size and angle. The POFACET also supports polar plot and linear plot. Finally, the Swirling model is designed for fluctuating RCS analysis.

Figure 1 shows the flow chart for the simulation of Radar cross section of different targets.

Overview of Radar Cross Section Analysis of Simple Objects and Simulation of Complex Objects

Sphere

The design equations for sphere are as mentioned in (Mahafza, 2005). The Fig. 2. clearly depicts the RCS of sphere for the three regions namely Rayleigh, Mie and Optical with respect to wavelength λ.

With further analysis using Radar toolbox, Table 1 shows the comparison of RCS of sphere for different radius keeping the frequency constant. It shows that RCS variation is dependent on frequency for smaller radius and for larger radius RCS remains constant and is independent of frequency.

The plots in Fig. 3a, 3b and 3c shows RCS for different radius and the same set of frequencies. For rad = 1 m and frequency in (GHz) = 1.3, 1.4, 2.5, 4.5, 9.5, the RCS value obtained is approximately the same in DBSM as Fig. 3. (c). Further analysis for *rad* = 2 m and frequency in (GHz) = 1.3, 1.4, 2.5, 4.5, 9.5, the RCS value obtained is 11 DBSM. Hence, RCS for a sphere is not wavelength -dependent.

In POFACET, the design and comparison for monostatic RCS for sphere of radius (r) 1 m and 2 m at a frequency of 1.4 (GHz) is done. The plot of Fig. 4a and Fig. 4b shows linear and polar plots at radius 1 m and frequency 1.4 (GHz). Similarly, for *rad* = 2 m and frequency 1.4 (GHz) the linear plot and polar plots is shown in Fig. 5a and 5b. The plot obtained by using POFACET and Radar toolbox reflects the same

characteristic for sphere. From the polar plot shown in Fig. 4b and 5b it can be concluded that RCS remains constant in all directions for a sphere.

Cylinder

I.RCS Pattern of Elliptic Cylinder

The backscattered RCS for elliptic cylinder is independent of azimuth direction. Using the Radar toolbox in MATLAB and Eq. (2), RCS is plotted for $r2 = 13$ cm and $r1 = 9$ cm, $h = 1$ m. As shown in Fig. 6, the RCS is maximum for f = 1.3 (GHz) and minimum for f = 4.5 (GHz) and f = 9.5 (GHz). It is observed that as frequency increases RCS return decreases. The maximum specular return occurs at 0° and reaches a minimum at 90°. The elliptic cylinder is converted to a circular cylinder making radius equal ($r1 = r2$) in Eq. (2).

$$\sigma\theta n = \frac{2\pi H^2 r(r2)^2 (r1)^2}{\lambda (r1)^2 (\cos\phi)^2 + (r2)^2 (\sin\phi)^2)^{1.5}} \tag{2}$$

In POFACET, the design and calculation of monostatic RCS for a circular cylinder of radius $r1 = r2 = 15$ cm, height(h) = 1 m at a frequency of 9.5 (GHz) is as shown in Fig. 7. The backscattered RCS is maximum for the central portion of the cylinder and minimum for the side portion of a cylinder as shown in Fig. 7a. The 3D-model design of the cylinder is as shown in Fig. 7a while the linear and polar plots are as Fig. 7b and 7c.

The RCS return is maximum at 180° when the cylinder is aligned horizontally about radar, while the minimum RCS is obtained at 90° and 270°.

Ellipsoid

The analysis of an ellipsoid using Eq. (3) in MATLAB is discussed. The backscattered RCS for an ellipsoid is independent of azimuth and elevation angle and depends only on the dimensions of the same. The Fig. 8a represents RCS of ellipsoid vs elevation angle with respect to dimensions. If all the three dimensions are equal then the RCS obtained is constant as sphere as shown with red line in Fig. 8a:

$$\sigma = \frac{\pi a^2 b^2 c^2}{\left(a^2 (\sin\theta)^2 (\cos\theta)^2 + b^2 \left(\sin\theta\right)^2 + c^2 (\cos\theta)^2\right)^2} \tag{3}$$

As the length of major axis c is reduced to half, the RCS is also reduced as shown in Fig. 8b with $c' = c/2$ and 8.(c) with $c' = c$. The value of RCS is maximum for larger value of c.

The design for monostatic RCS of ellipsoid for $a = 25$ cm, $b = 30$ cm, $c = 1$ m at frequency of 4.5 (GHz) is done using POFACET as shown in Fig. 9a. The 3D -

model design of an ellipsoid is shown in Fig. 9a. The backscattered RCS is maximum at 90° and 270° from linear plot shown in Fig. 9. (b) and polar plot in Fig. 9. (c).

Triangular Flat Plate

The triangular flat plate is defined by the ideal case of isosceles triangle when oriented at center for RCS measurement. Using Eq. (4), (5) and (6) backscattered RCS is calculated at angle 30°.The combined RCS plot for the frequency $f = 1.3$, 4.5 and 9.5 (GHz) and for the dimension $a = 0.2$ m and $b = 0.75$ m is shown in Fig. 10. As the frequency increases the RCS obtained varies with high fluctuations:

$$\sigma = \frac{4\pi A^2}{\lambda^2} (\cos\theta)^2 \sigma_0 \tag{4}$$

$$\sigma_0 = \frac{\left[(\sin a)^2 - \left(\sin^2\left(\frac{\beta}{2}\right)\right)\right]^2 + \sigma_{01}}{\alpha^2 - \left(\frac{\beta}{2}\right)^2} \tag{5}$$

$$\sigma_{01} = 0.25(\sin\phi)^2 \left[\left(2\frac{a}{b}\right)\cos\phi\sin\beta - \sin\phi\sin 2\alpha\right]^2 \tag{6}$$

$$where\ \alpha = k\alpha\sin\theta\cos\phi, \beta = kb\sin\theta\sin\phi\ \&\ A = ab/2.$$

The triangular plate model is designed manually in POFACET with co-ordinates shown in Table 2. For a = 0.2 m and b = 0.75 m, the calculated monostatic RCS for elevation angle approximately at 30° and frequency 4.5 (GHz) is shown in Fig. 11. (a). The backscattered RCS is the backscattered RCS is maximum at the edges as shown in Fig. 11. (a) with 3D RCS model of plate. The linear and polar plots show RCS are maximum at 0° and 180 ° as shown in Fig. 11. (b) and 11. (c).

Circular Flat Plate

A circular flat plate is defined for radius r. Analysis is done using Eq. (7). The RCS return of a circular flat plate at different frequencies are plotted in Fig. 12. (a), 12. (b), 12. (c), 12. (d) ,12 (e), for radius (r) = 30 cm and 12. (f) for $rad = 45$ cm and $f = 9.5$ (GHz). Figure 13 represents combine plot of all the RCS return at different frequency for $rad = 30$ cm which is highly fluctuating.

$$\sigma = \frac{4\pi^3 r^4}{\lambda^2} For\theta° \tag{7}$$

As frequency and radius varies RCS of flat plate varies. Hence, circular flat plate represents highly fluctuating target.

Table 1: Comparison of Backscattered RCS of sphere for different frequencies and radius.

Frequency (GHz)	RCS (DBSM)		
	Rad = 20 cm	Rad = 30 cm	Rad = 1 m
$f = 1.3$	-10.29	-5.07	4.88
$f = 1.4$	-7.97	-5.89	4.92
$f = 2.5$	-9.02	-5.21	4.95
$f = 4.5$	-9.10	-5.6	4.95
$f = 9.5$	-8.96	-5.5	4.97

Table 2: Code for triangular plate in POFACET

x	y	z
0.20	0	0
0	0.375	0
0	-0.375	0
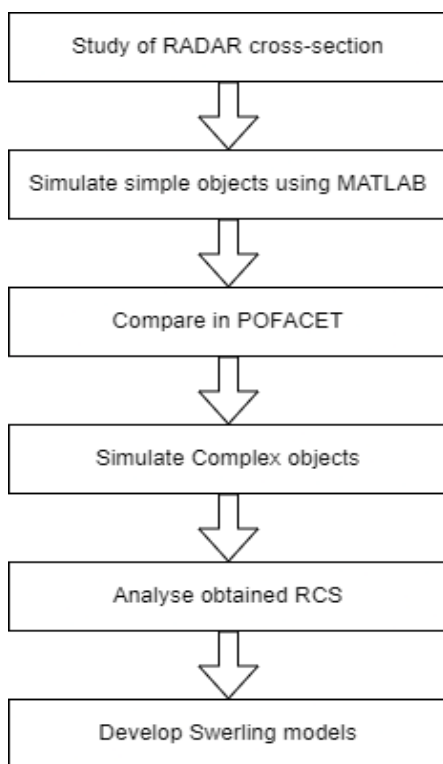
Fig.1: Flow chart for RCS simulation
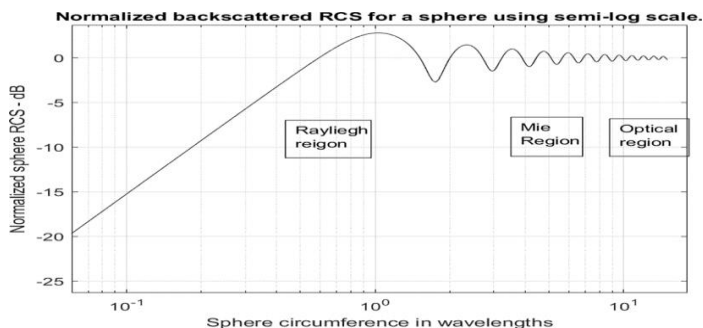
Fig. 2: Normalized RCS of sphere   for all the three regions with respect to λ

4
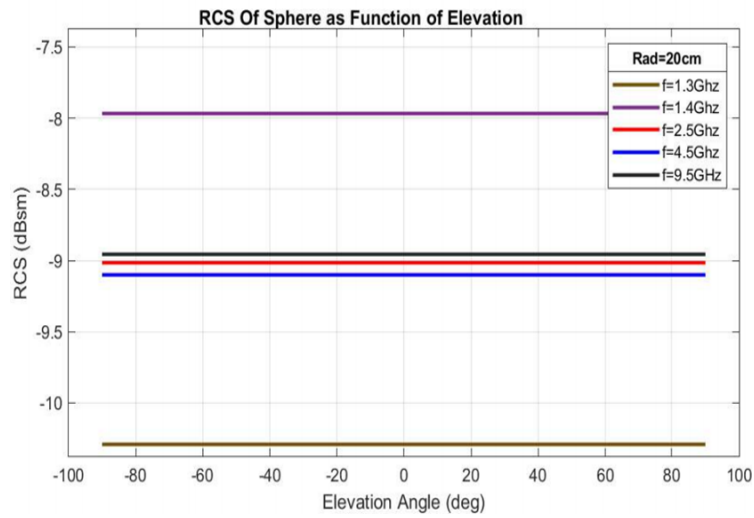
(a)
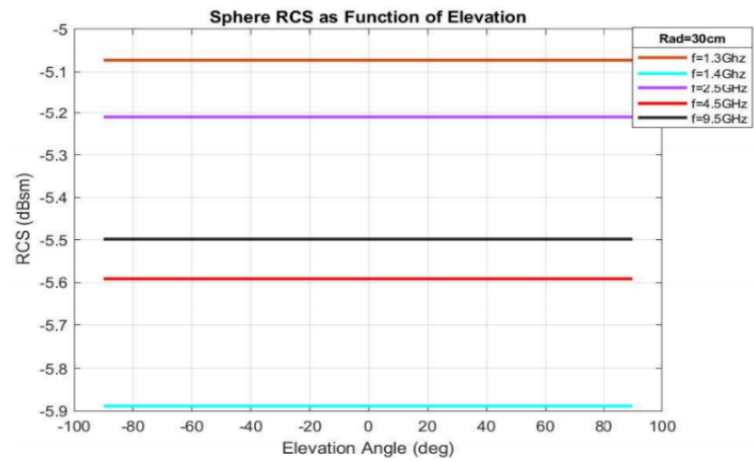
(b)
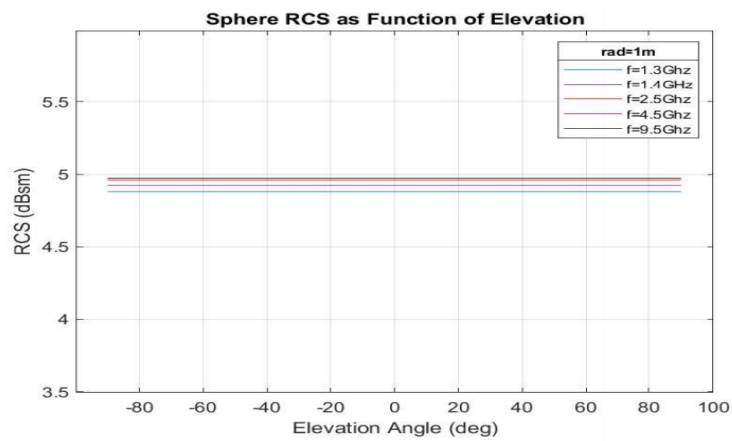
(c)

Fig. 3: (a) RCS of Sphere as a function of elevation for different frequencies for rad = 20 cm; (b) RCS of Sphere as a function of elevation for different frequencies for rad = 30 cm; (c) RCS of Sphere as a function of elevation for different frequencies for rad = 1 m
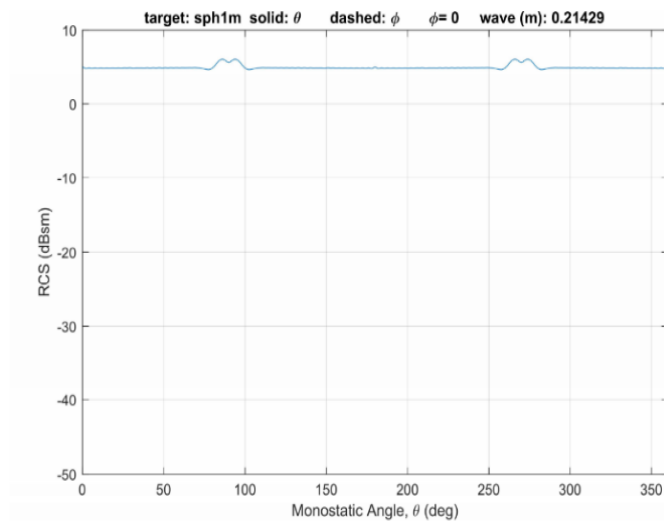
(a)
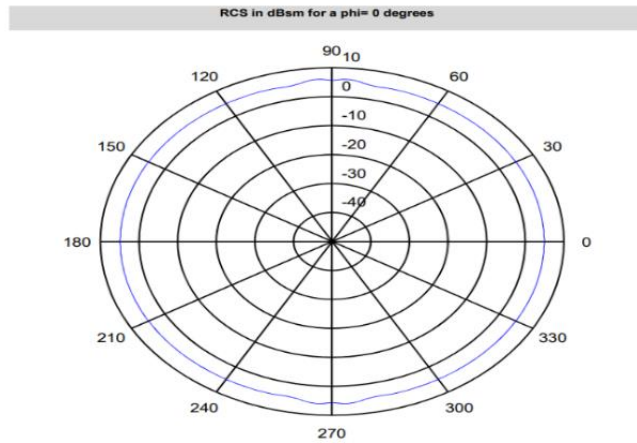
(b)

Fig. 4: (a) Linear plot for sphere rad = 1 m, f = 1.4 (GHz); (b) Polar plot for sphere, rad = 1 m, f = 1.4 (GHz)

(a)

(b)
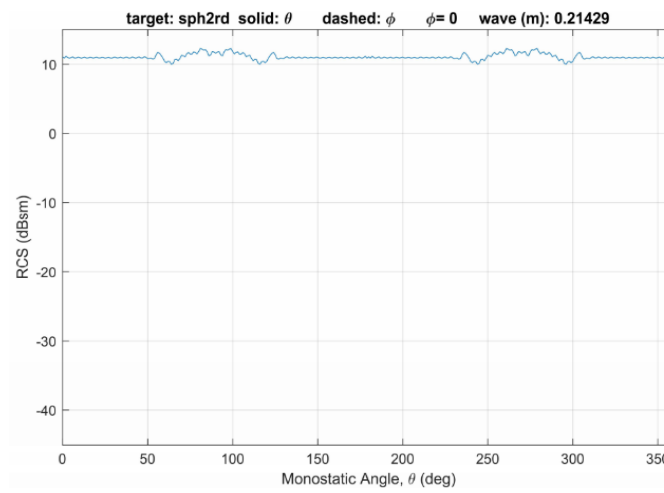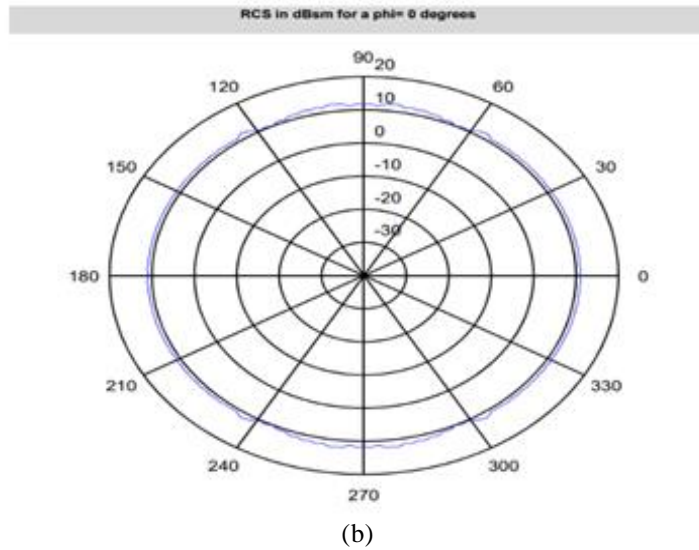
Fig. 5: (a) Linear plot for sphere rad = 2 m, f = 1.4 (GHz); (b) Polar plot for sphere rad = 2 m, f = 1.4(GHz)
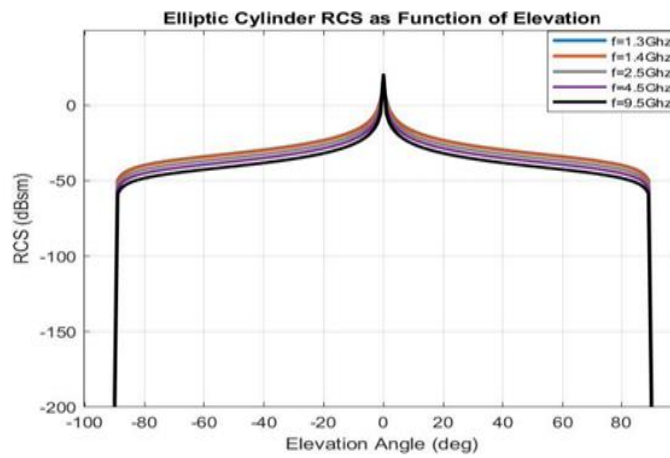
Fig. 6: RCS pattern of Elliptic Cylinder. r_2 = 13 cm, r_1 = 9 cm, h = 1 m

(a)

7
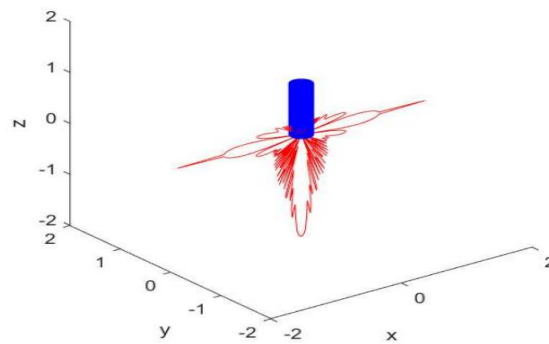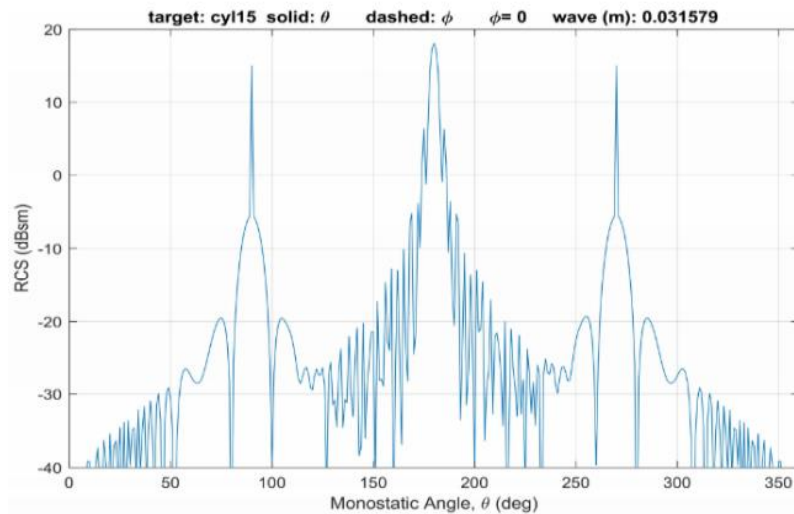
(b)
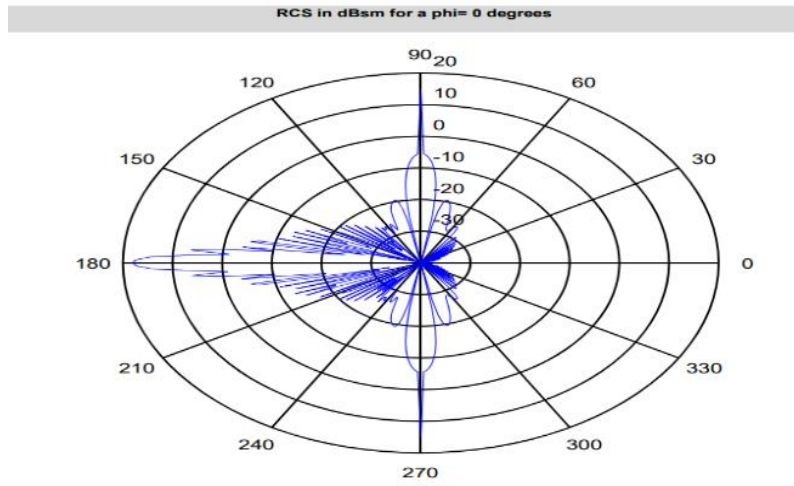
(c)

Fig. 7: (a) 3D- model for monostatic RCS of cylinder for $r_1 = r_2 = 15$ cm, h = 1 m at f = 9.5 (GHz); (b) Linear plot RCS of cylinder; (c) Polar plot RCS of cylinder
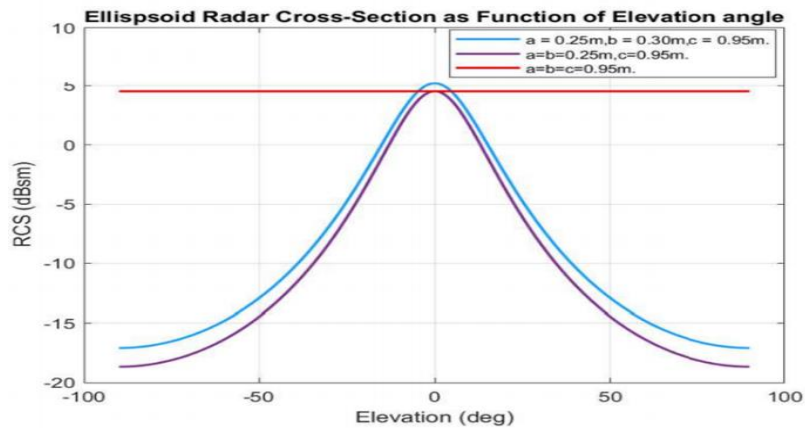
(a)
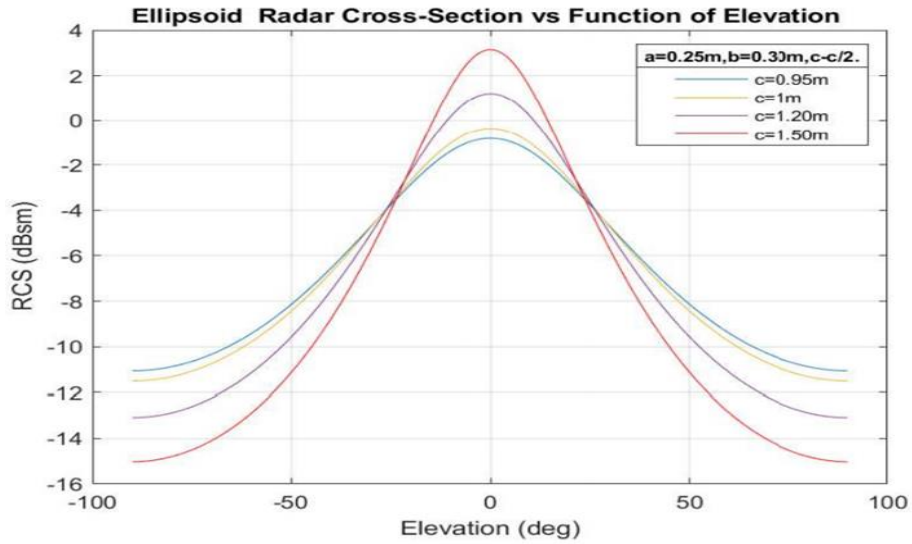
(b)
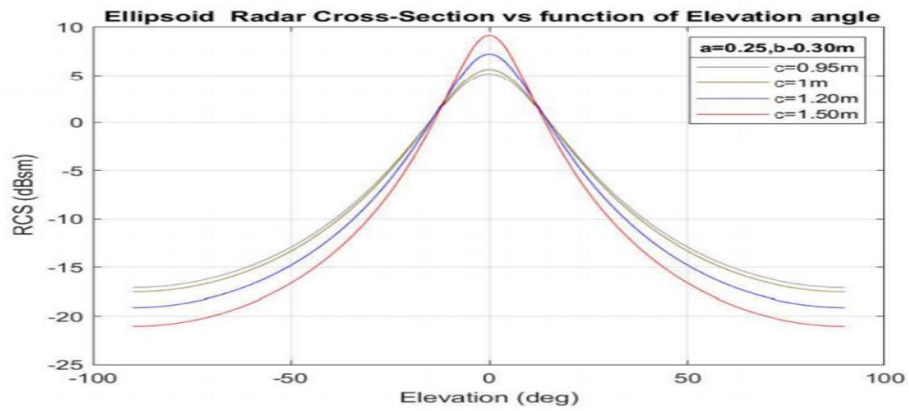
(c)

Fig. 8: (a) RCS pattern of ellipsoid vs Elevation, for a, b, c dimensions; (b). RCS pattern of ellipsoid vs Elevation, for a = 25 cm, b = 30 cm, c'= c/2; (c). RCS pattern of Ellipsoid vs Elevation, for a = 25 cm, b = 30 cm, c' = c

(a)

9
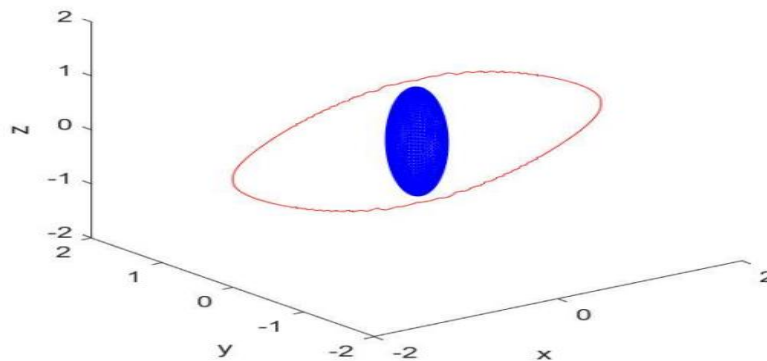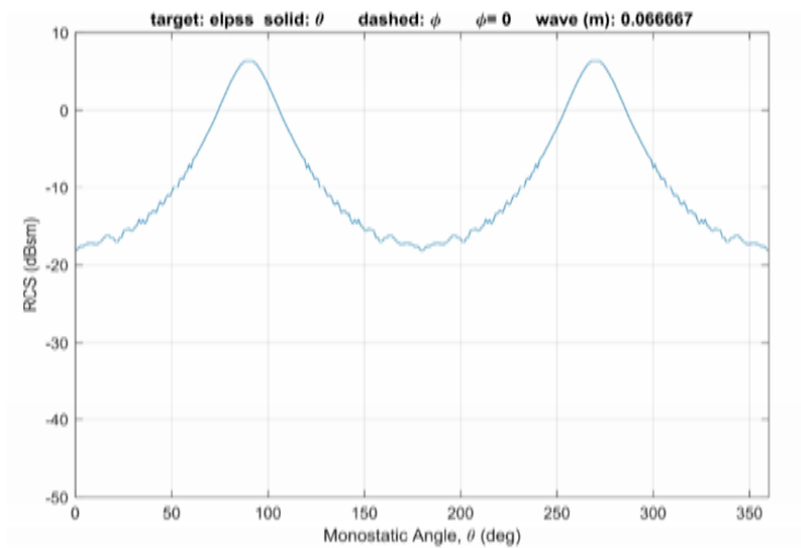
(b)
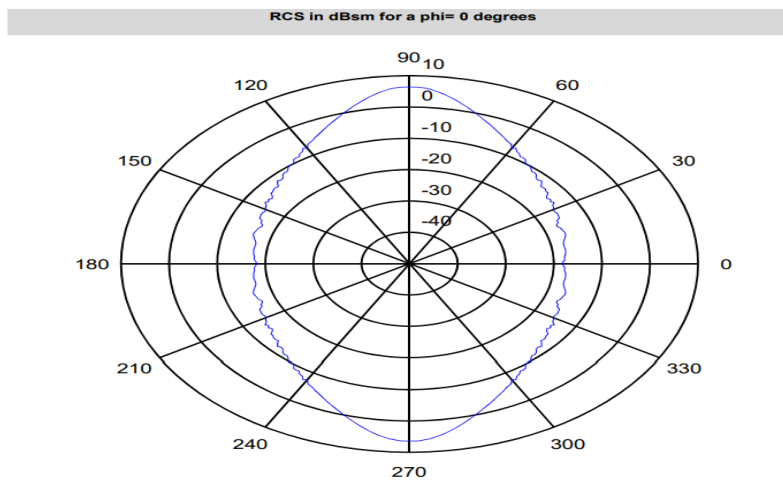
(c)

Fig. 9: (a) 3D- model of ellipsoid for a = 25 cm, b = 30 cm, c = 1 m at f = 4.5 GHz; (b). Linear plot monostatic RCS of ellipsoid; (c). Polar plot monostatic RCS of ellipsoid
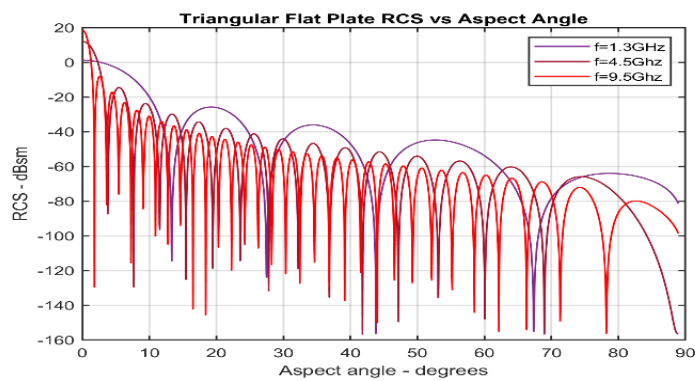
Fig. 10: RCS return plot of a perfectly conducting isosceles triangle plate, a = 0.2 m and b = 0.75 m

10

Truncated Cone (Frustum)

The truncated cone (frustum) is defined by the half cone angle $\propto$ measured by Eq. (8) and backscattered RCS is calculated by using Eq. (9). The variation of RCS with elevation angle for a truncated cone target for different values of frequency is plotted in Fig. 14. (a) and Fig. 14 (b), with the top radius ($r2$), the bottom radius ($r1$) and height (h).

$$\tan a = \left(\frac{r2 - r1}{h} \right) = \frac{r2}{l} \tag{8}$$

$$\sigma\theta_n = \frac{8\pi \left(z_2^{3/2} - z_1^{3/2} \right)^2 \sin a}{9\lambda(\cos \alpha)^4} \tag{9}$$

From Fig. 14a and 14b, the RCS has maximum & minimum values at aspect angles of 0° & 80°. The RCS is maximum depending on the frequency, whereas it decreases with an increase in the frequency. From Fig. 14a, at $h = 1.20$ m RCS obtained will be maximum. Similarly in Fig. 14b RCS is maximum for height h=1m for different dimensions of a truncated cone.

RCS of Complex Objects:

For complex objects, RCS is contributed by summing the individual RCS of each shape. Fig 15a shows the 3D model design of the circular cylinder.

The plot for the circular cylinder with a flat plate on both sides is shown in Fig. 15a with $h = 2$ m, $r = 0.50$ m and $f = 9.5$ (GHz). From Fig. 15b the RCS return is maximum due to cylinder and minimum from flat plates.

Figure 16a shows a model of the ellipsoid with a circular cylinder with a flat plate at both ends. The RCS plot obtained for the ellipsoid is added vectorially with the circular cylinder and flat plate using Eq. (3), (10), (11) and (12), as Fig. 16b. The RCS obtained for this designed model is maximum at aspect angle of 0 degree and 180 degrees. The RCS obtained is minimum in the aspect angle range of 60 to 120 degrees.

Circular Flat Plate

$$\sigma = \frac{\lambda r}{8\pi \sin(\theta)(\tan(\theta))^2} \tag{10}$$

$$\sigma = \pi K^2 r^4 \left(\frac{2/1(Krin\theta)}{2Kr\sin\theta} \right)^2 (\cos\theta)^2 \tag{11}$$

Here, K = $2\pi/\lambda$ and $J_{(1)}(\beta)$ is the first order spherical Bessel function evaluated at $\beta = Krsin\,\theta$.

Cylinder

For normal incidence:

$$\sigma\theta_n = \frac{2\pi H^2 r}{\lambda} \tag{12}$$

An example of a frustum and flat plates is as shown in the Fig. 17a, for X- band radar is situated at the left side of the object. The RCS is obtained using Eq. (8), (9) for small end to large end of frustrum and Eq. (7) for flat plates at normal incidence Fig. 17b shows RCS of frustum without flat plate. Fig. 17c shows the RCS vs aspect angle plot for a frustrum with flat plates on both ends while the radar is positioned at normal incidence of the small end. The radius of both ends of the frustrum is the same as the radius of the flat plates. The maximum RCS obtained is due to frustum and minimum due to flat plates and the normal incidence occurs at 73.3008° as depicted in the Fig. 17c.

For X- band radar situated at the left side of the object with normal incidence. The model for half ellipsoid and frustum with flat plates at a frequency 9.5 (GHz) is shown in Fig. 18a using Eq. (3), (7), (8) and (9). The values considered for half ellipsoid at incident angle of 90 ° are $a = 0.05$ m, $b = 0.10$ m, $c = 0.15$ m, *phi* = 90; and for frustum with flat plates are $r1 = 0.075$ m, $r2 = 0.225$ m, frequency = 9.5 GHz, height = 0.50m. The plot for RCS vs aspect angle is from small end to large end shown in Fig. 18b.

Swerling Models

Practically in radar applications, the targets are moving, having relative motion with radar. Radar cross-section varies slowly or rapidly with targets characteristics. The calculated RCS fluctuates for a specific period as a function of frequency and target aspect angle. This fluctuating RCS is termed as dynamic radar cross section of target. Dynamic RCS varies with amplitude or phase in a given scan. The RCS of simple shape objects is also very complex sometimes. Hence, the complex targets RCS is measured by statistical modeling.

The Swerling model is an example of a statistical model. The American Mathematician, Peter Swerling had first introduced the Swerling models in 1954. The statistical model involves time correlation properties of measured RCS Richards (2005). The probability density function with Chi-Square of degree given by Eq. (13) is used to study models based on average RCS:

$$f(\sigma) = \frac{m}{\Gamma(m)\sigma av} \left(\frac{m\sigma}{\sigma av} \right)^{m-1} e - \frac{m\sigma}{av} \sigma \geq 0. \tag{13}$$

where, $\Gamma(m)$ is gamma function in argument m ,and σ_{av} is the average RCS in the overall fluctuation . As degree increases RCS values have narrow range. For $\sigma \rightarrow \infty$, the target is static

The Swerling models for the fluctuating RCS are illustrated in the following example. The monostatic radar and object are considered stationary for explaining both Swerling model II and IV in the given study.

Design Specifications

(1) The radar beam scans for 5secs in one rotation of 360°. Hence scan rate is 72 rates per sec

(2) HPBW (Half power beam- width) = 3°, which is the major beam incident on the target. The target focused by the beam for a specific period is called dwell time or scan time. The number of scans is 3

(3) Pulse Repetition Frequency (PRF) is number of pulses sent during dwell time and is assumed to be 5000 Hz

(4) Number of pulses = Dwell time *PRF

(5) Swerling model I, II, III and IV have been created by applying the step method using MATLAB

(6) The radar antenna is set up with transmitting frequency $fc = 1.3$ (GHz) and initial location at [0,0,0] while target is positioned at 4000 m

(7) PW (Pulse width) = 50*10^-6

(8) The transmitting amplifier in radar transmits with linear FM (Frequency modulation), with peak power = 1.5kW and Gain = 40

(9) The mean RCS $\sigma = 1.2$ value is set up for both

Swerling model II and IV

(10) The following results are obtained by performing the analysis on radar receiver and matched filter

(11) The radar collects the return amplitudes which are plotted against time for the specified model

Figure 19 shows the plot of Swerling models I and II with the above data. The RCS obtained for this model is the amplitude of the received pulse varying with time. The model obeys the Chi-square distribution Probability Density Function (PDF) with a degree of freedom 2. Swerliang models I and II are interchangeable within a scan. The RCS amplitude obtained is constant with time or is equal to the sum of independent small scatters. Similarly, the Swerling models III and IV are plotted in Fig. 20. The total RCS amplitude obtained consists of one large scattering surface and a small scattering surface within a pulse. The statistical model obeys Chi-square PDF with a degree of freedom 4. The measured RCS of high-speed debris revolving around the earth's surface by the radar in Low Earth Orbit (LEO) orbit can be modeled as Swerling models.

3D RCS Plot of trpl1 Model: RED:RCS-θ, GREEN:RCS-ϕ

(a)

(b)

(c)
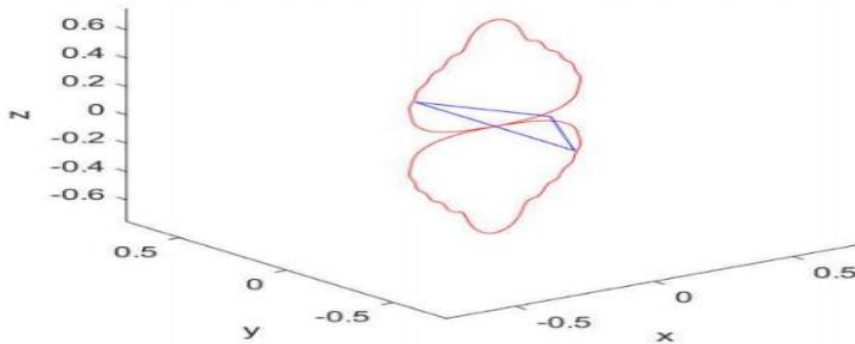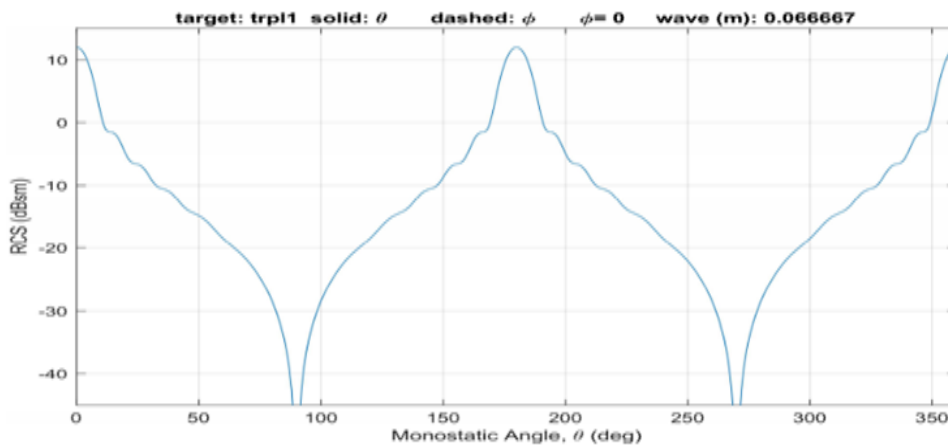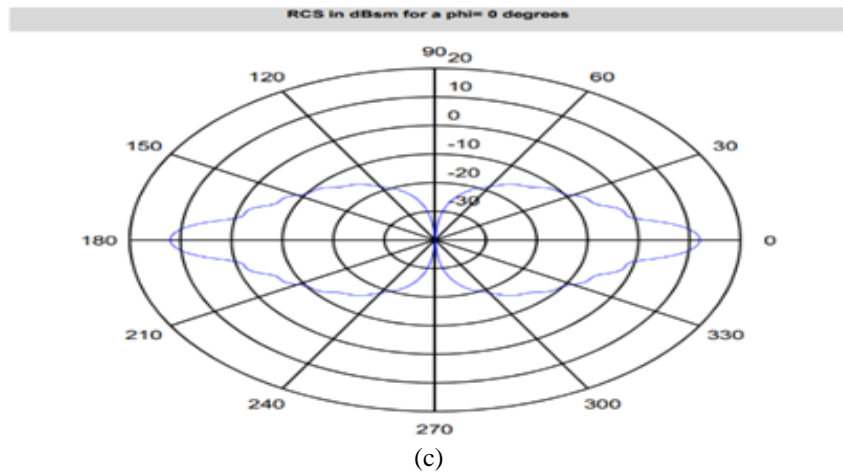
Fig. 11: (a) 3D- model Triangular plate monostatic RCS for elevation angle approx. 30 deg at 4.5 Ghz; (b): Linear plot monostatic RCS of Triangular plate; (c): Polar plot monostatic RCS of Triangular plate

(a)

(b)

13
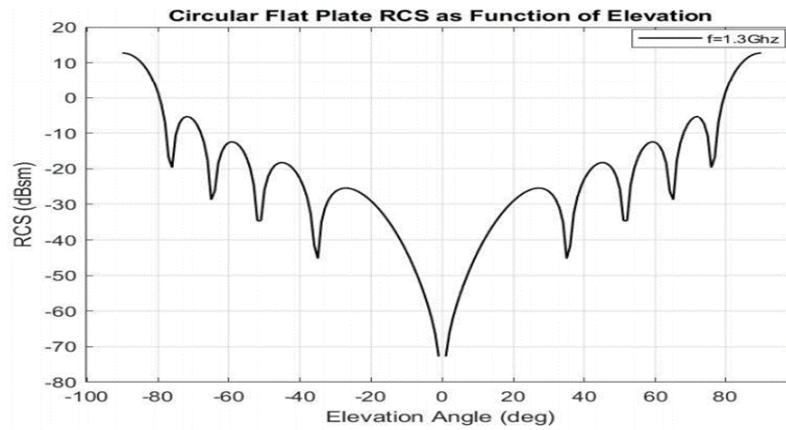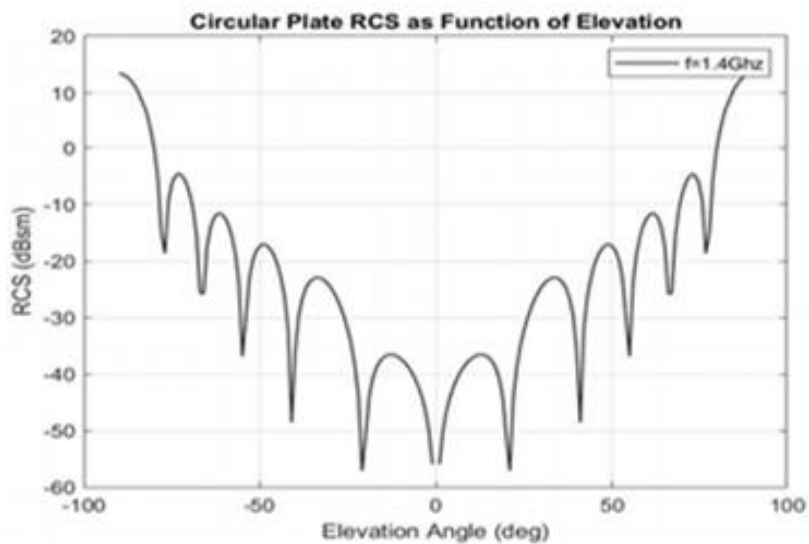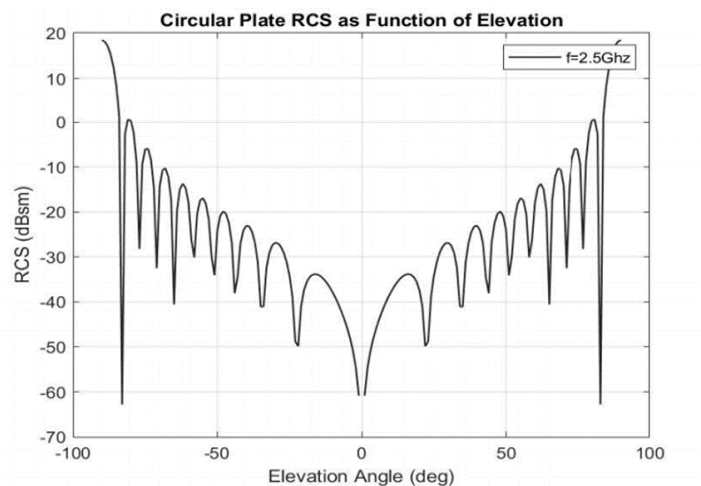
(c)
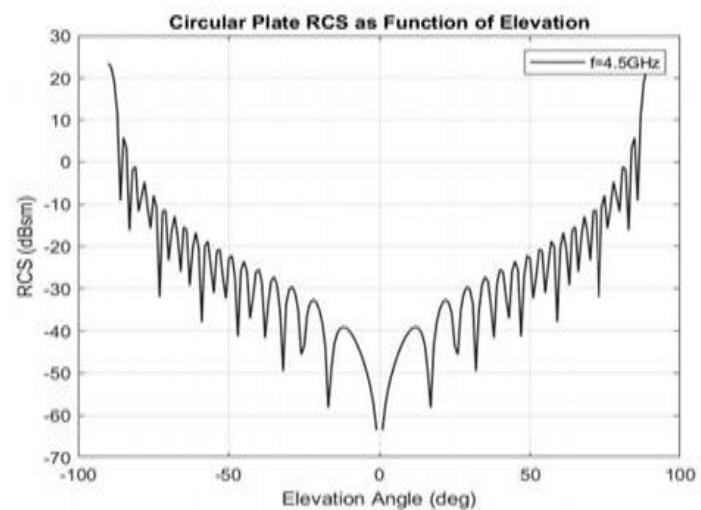
(d)
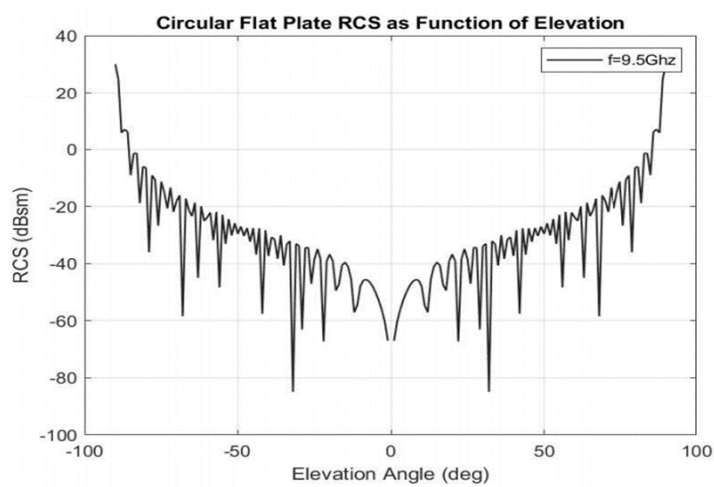
(e)
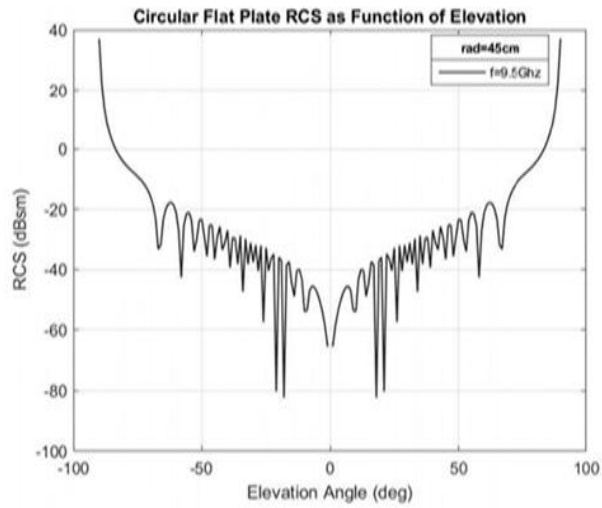
(f)

Fig. 12: (a) RCS of Circular Plate -f = 1.3 (GHz), r = 30 cm; (b). f = 1.4 (GHz), r = 30 cm; (c). RCS return plot of Flat Circular Plate: f = 2.5 (GHz), r = 30 cm; 12 (d). f = 4.5 (GHz), r = 30 cm; (e) RCS return plot of Flat Circular Plate: f = 9.5 (GHz), r = 30 cm; (f). f = 9.5 (GHz)
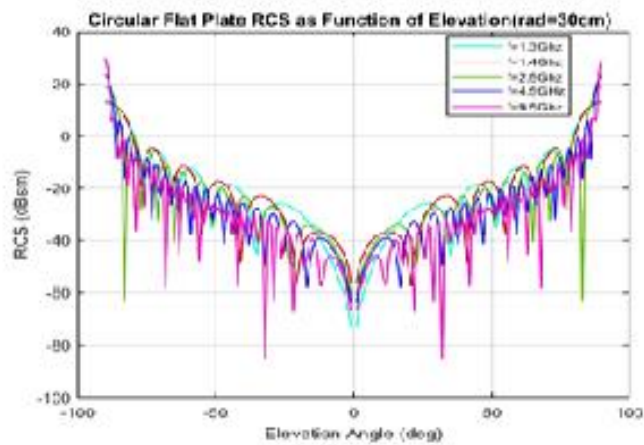
Fig. 13: Combine backscattered RCS plot of Flat Circular Plate: radius = 30 cm

(a)

15

(b)
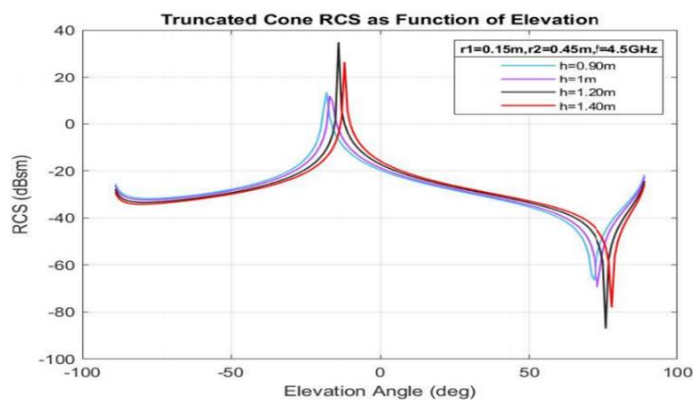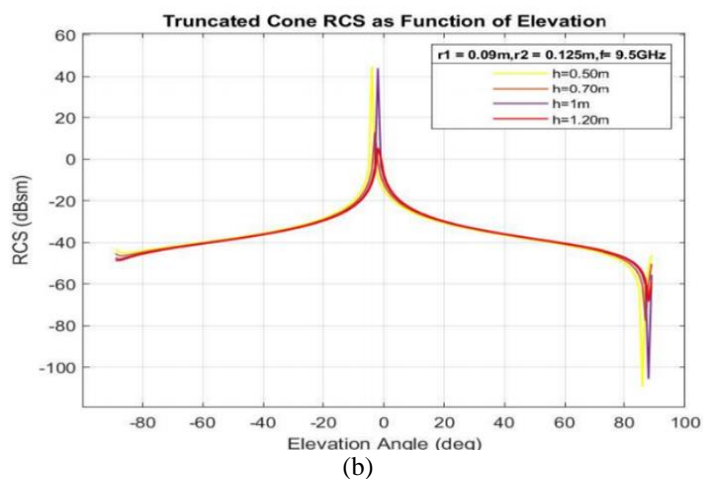
Fig. 14: (a) Backscattered RCS of Truncated cone: fc = 4.5 (GHz), r1 = 15 cm, r2 = 45cm with varying 'h; (b) Backscattered RCS of Truncated cone fc = 9.5 (GHz); r_1 = 9 cm; r_2 = 12.5 cm with varying 'h'

(a)
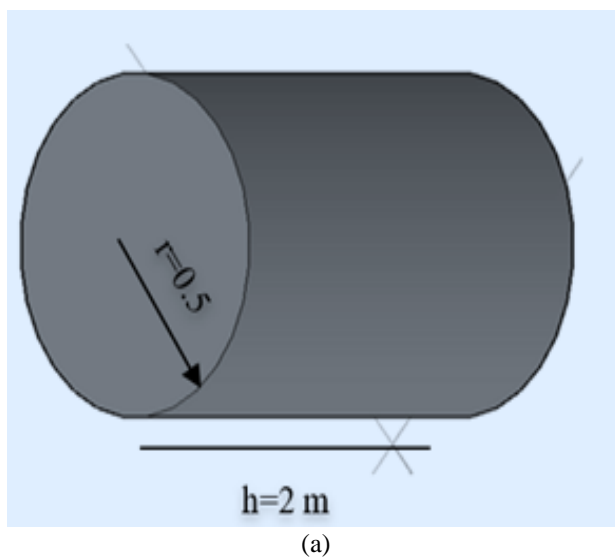
Fig. 15: (a) 3D-model of cylinder; (b) RCS obtained of a circular cylinder with two flat plates on both sides

(a)
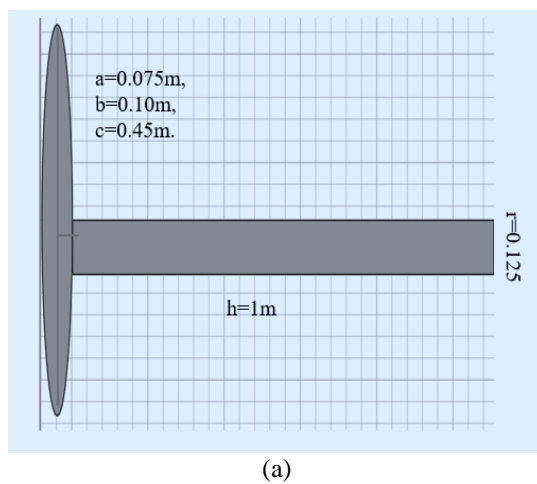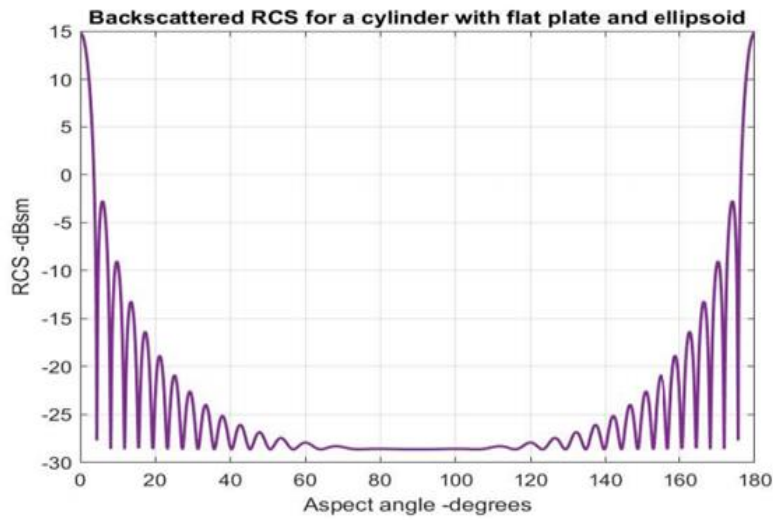
(b)

Fig. 16: (a) Model for ellipsoid with cylinder; 16. (b)A circular cylinder with flat plates h = 1 m and r = 0.125 m and   ellipsoid a = 0.075 m; b = 0.10 m; c = 0.45 m and f = 9.5 GHz

(a)

(b)

17

(c)
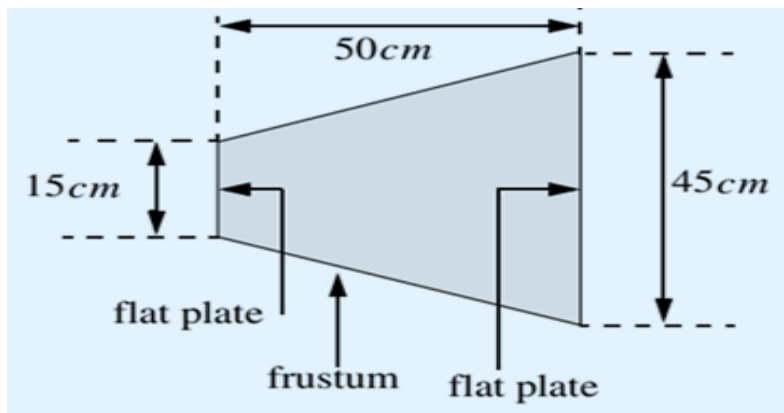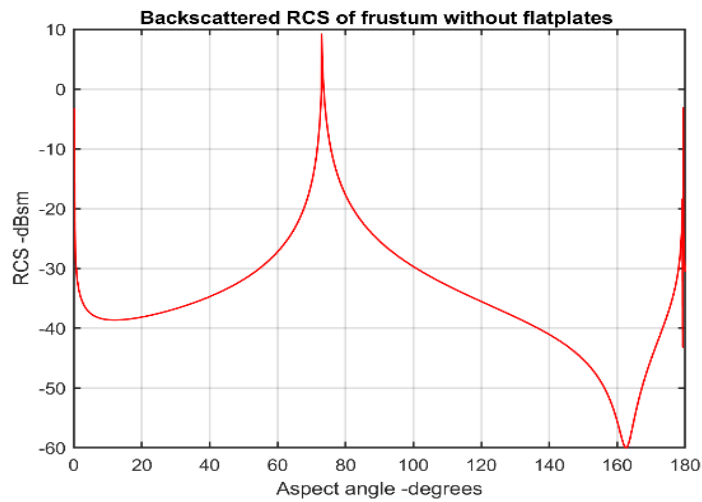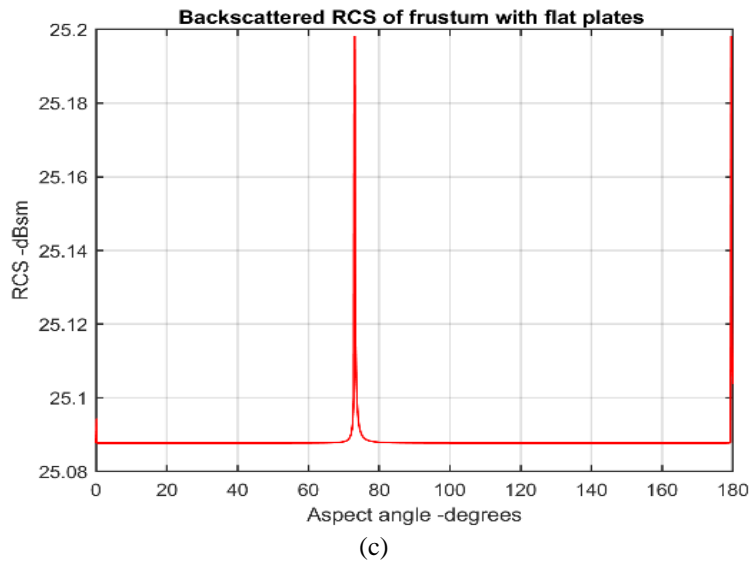
Fig. 17: (a) Model for frustrum with flat plates at both ends; (b): RCS of frustum without flat plate; (c) RCS plot for $r_1 = 0.075$ m, $r_2 = 0.225$ m, h = 0.50 m, h = 0.50 m, f = 9.5 (GHz). Viewing form small end to large end

(a)

(b)
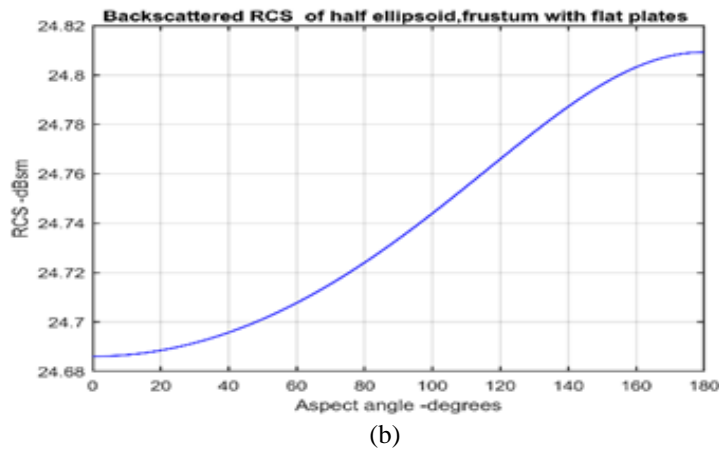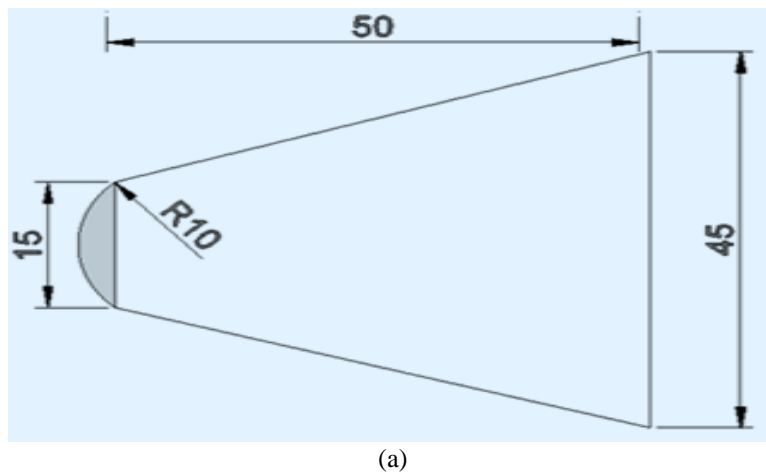
Fig. 18: (a) Model for half ellipsoid and frustrum with flat plates; (b) RCS vs aspect angle plot
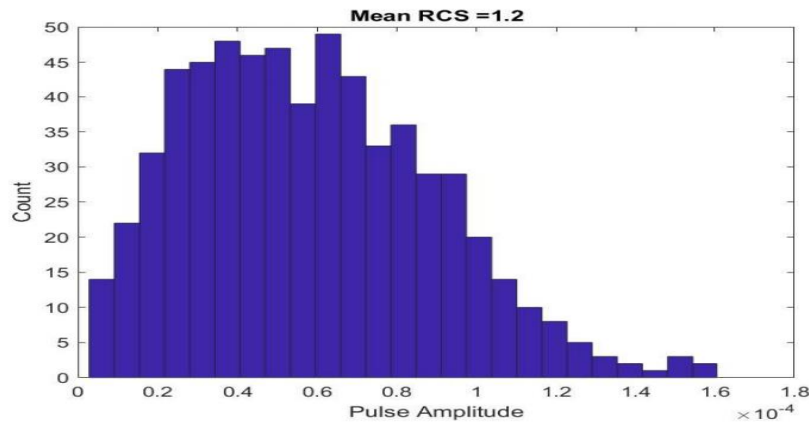
Fig. 19: Histogram plot of received amplitude for Swerling target models I and II
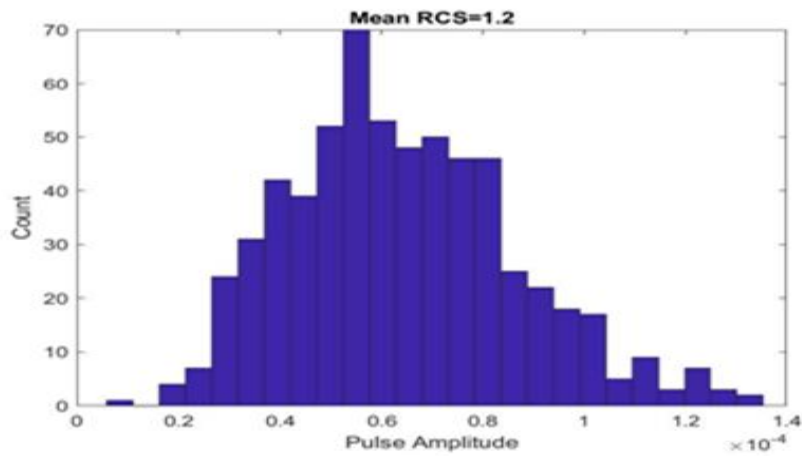
Fig. 20: Histogram plot of Swerling target models III and IV with mean RCS $\sigma = 1.2$

Table 3: Measured RCS for complex objects:

Complex objects	RCS calculated
1.For complex cylinder with flat plates	25.998 DBSM at Normal incidence
2.An ellipsoid with flat plates and cylinder	14.69 DBSM from rare ends
3. A Frustum without flat plates	9.99 DBSM from small end to large end.
4.A frustrum with Flat plates at both ends.	25.09 DBSM at 0°, 25.19 DBSM at 73.008°, 25.19 at 180°.
5.A half - ellipsoid with frustum and flat plate	24.80 DBSM at 180°.

Conclusion

In this study, RCS measurement of simple objects are thoroughly reviewed for new design of complex object using MATLAB simulation and Physical Optics method. The statistical analysis of RCS is very useful and promising for high-speed rotating targets.

The RCS of sphere is constant for high values of radius and varies for low value of radius. Hence, the RCaS of the sphere is dependent on the radius and size of the sphere and independent of frequency. The cylinder and ellipsoid share the maximum specular return at 0°or 90°.The triangular plate and circular flat plate have a highly fluctuating RCS. For truncated cone, RCS is maximum at 0° and minimum at 80°. RCS also varies with frequency and height for the truncated cone. For any complex object the vectorial addition of simple object gives the RCS. For a complex object like circular cylinder mounted with two perfectly conducting circular flat plates at both ends, the RCS is contributed by cylindrical surface at 90°. At 0°and 180° the RCS is contributed by the circular flat plate. The RCS is

contributed only from end points from a circular cylinder mounted with ellipsoid at one end. The model of frustum with circular flat plates gives maximum specular return at 73.3008° . The RCS plot for half-ellipsoid with frustum and flat plates increases from 0° and reaches maximum at 180°.A comparative study has been done of the basic models with POFACET GUI. The RCS modelling of a fluctuating target is done using Chi-square degree distribution for Swerling models II and IV. The detailed analysis of Swerling models for the fluctuating RCS will be applicable to measure RCS of high-speed debris revolving around the earth's surface by the radar in Low Earth Orbit (LEO). The detailed study of modelling will be also applicable in determining the RCS of unknown complex objects by analyzing simple objects. This type of RCS modelling will be useful in analysing the structure of unknown targets related with applications such as military, defence and space debris in Lower Earth Orbit (LEO).

The future scope is to study RCS of the real objects used in the underwater and satellite communication. This work may be extended to military, defence and space debris in low earth orbit and also specific geometries such as ships, planes.

Acknowledgement

Author's Contributions

Punam Pande: Simulation and Implementation of the results.

R. Sreemathy and Mousami Turuk: Technical and Research Guidance, Verification of the results, Drafting and Revision of the manuscript.

Ethics

This article is original and contains unpublished material. The corresponding author confirms that all other authors have read and approved the manuscript and no ethical issues have been involved

References

Afrazi, M., Pirjalili, A., Golshani, A. A., & Fakhournezhad, A. (2017). MATLAB codes for finite element analysis of a tunnel. In Proceeding of the 4th International Conference on Recent Innovations in Civil Engineering, Architecture and Urban Planning, Tehran, Iran, September.

Ahmed, T. I. O., & Mirghani, M. (2018). Estimation of Radar Cross Sectional Area of Target using Simulation Algorithm. International Journal of Research Studies in Electrical and Electronics Engineering, 4(2). https://www.joseheras.com/pdfs/ijrseee/v4-i2/3.pdf

Chibuisi, I. (2015) Simulation of Radar Cross Section (RCS) of Spherical Objects. http://www.ijtrd.com/papers/IJTRD226.pdf

Divyalakshmi, A., Bhuvana, A., & Babu, G. V. (2018). Analysis of radar cross section and detection". International Journal of Pure and Applied Mathematics. No. 16, 2018, 119, pp-469-477.

Emhemmed, A. S., Shebani, N., Zerek, A., & Ahmed, N. (2019, March). Analysis of RCS and Evaluation of PO Approximation's Accuracy for Simple Targets. In 2019 19th International Conference on Sciences and Techniques of Automatic Control and Computer Engineering (STA) (pp. 666-669). IEEE. doi.org/10.1109/STA.2019.8717195

Mahafza, B. R. (2005). Radar systems analysis and design using MATLAB. Chapman and Hall/CRC. doi.org/10.1201/9781420057072

Merrill, I. S. (2001). Introduction to radar systems. Mc Grow-Hill, 7(10).

Richards, M. A. (2005). Fundamentals of radar signal processing. Tata McGraw-Hill Education.

Shin, H., Yoon, D., Kim, C., Yang, Y. S., Lee, M. G., Park, J. Y., ... & Park, Y. B. (2021). Shape Optimization of an Integrated Mast for RCS Reduction of a Stealth Naval Vessel. Applied Sciences, 11(6), 2819. doi.org/10.3390/app11062819

Skolnik, M. I. (1970). Radar handbook. https://trid.trb.org/view/49654

Surender, V., Reddy, P. S., & Reddy, P. R. (2021, February). Dynamic RCS Modelling of Launch Vehicle Prior to Launch for Estimation of Real-time SNR. In Journal of Physics: Conference Series (Vol. 1804, No. 1, p. 012168). IOP Publishing. https://iopscience.iop.org/article/10.1088/1742-6596/1804/1/012168/meta?gridset=show

Xu, Y. L., Kennedy, T., & Stansbery, E. (2019, December). Radar Cross Section of orbital debris objects. In International Orbital Debris Conference (IOC) (No. IOC 6164). https://ntrs.nasa.gov/citations/20190033903